Met. Mater. Int., Vol. 17, No. 3 (2011), pp. 397~402
doi: 10.1007/s12540-011-0615-0 Published 29 June 2011

Fatigue Crack Propagation Behavior of AZ31 Mg Alloy in Ultra-High Vacuum

KyoSoo Song*, Hwa Chul Jung and Kwang Seon Shin

Magnesium Technology Innovation Center, Research Institute of Advanced Materials
School of Materials Science and Engineering, Seoul National University
599 Gwanak-ro, Gwanak-gu, Seoul 151-744, Korea

(received date: 15 September 2010 / accepted date: 31 December 2010)

The fatigue crack propagation (FCP) behavior of extruded AZ31-F was examined in conjunction with crack closure phenomena. FCP experiments were carried out in an ultra-high vacuum system using a fatigue test machine under a constant load amplitude. To determine the effect of crack closure on the FCP rates, the crack closure levels were measured using the compliance method. The ΔK_{th} values of the AZ31-F decreased with increasing load ratio. It was found that $\Delta K_{eff,th}$ showed an almost constant value regardless of the load ratio.

Keywords: alloys, extrusion, fatigue, crack closure, vacuum

1. INTRODUCTION

Mg alloys have several distinct advantages as structural materials, such as low density, high specific strength, acceptable ductility, and vibration dampening characteristics [1-4]. When using Mg alloys as structural materials, it is very important to understand their fatigue characteristics [5]. After the Paris-Erdogan equation of fatigue crack propagation (FCP) rate was introduced, many studies on the three regimes were carried out, and their respective FCP mechanisms were examined [6]. Most studies on FCP behavior focused on the Paris region, in which FCP rates are much faster than those in the near-threshold region. In general, however, the majority of the fatigue life will be spent at the crack initiation stage. Thus, if the fatigue life is predicted on the basis of the Paris equation, the resulting design could become very conservative due to the presence of the threshold region. To solve this problem and to achieve effective structural design, it is necessary to examine the FCP behavior in the near-threshold region. It has been reported that the FCP behavior in the near-threshold region is very sensitive to factors including the load (R) ratio, microstructure, test environment, and especially crack closure phenomena [7,8].

Although studies on the fatigue behavior of Mg alloys are increasing these days, it is still at an initial stage when compared with studies on Al alloys, which are the most widely used lightweight structural materials [9,10]. In addition, most of these studies are conducted in aggressive environments, such as humid air and sodium chloride solution. Nan *et al.* reported that the corrosion fatigue lives of AZ31 decreased compared with those in laboratory air [11]. Kobayashi *et al.* studied the environmental effect on the FCP behavior of AZ91 in dry and wet Ar and air, and found that the FCP behavior strongly depends on the test environment [12]. To understand the mechanism of FCP behavior in the absence of environmental effects, it is necessary to conduct FCP tests in high vacuum conditions [13], but there have only been very limited studies on the FCP behavior of Mg alloys in a vacuum up to now [14-16].

The objective of the present study is to examine how crack closure affects the FCP behavior of extruded AZ31, which is one of the most widely used Mg alloys, with various R ratios in an ultra-high vacuum system, especially in the near-threshold region.

2. EXPERIMENTAL PROCEDURES

2.1. Specimen preparation

The material used in the present study was the AZ31-F alloy, and the chemical compositions are listed in Table 1. A Mg ingot with a 180 mm diameter was cast, and was subsequently extruded by a 1,800 ton extrusion machine, at an extrusion ratio of 25:1 to have a cross section of 80 mm × 12.5 mm. AZ31-F exhibits elongated grains along the extrusion direction, and the average grain size was 18 μm. Cylindrical tensile specimens were machined from the center portion of the plate, and tensile tests were carried out at room

*Corresponding author: sks0228@snu.ac.kr

Table 1. Chemical compositions of the AZ31-F alloy

Alloy	Al	Zn	Mn	Si	Fe	Cu	Ni	Mg
AZ31	3.39	1.10	0.59	0.007	0.004	0.003	0.001	Bal.

Table 2. Mechanical properties of the AZ31-F alloy

Alloy	Yield Strength (MPa)	Tensile Strength (MPa)	Elongation (%)	Young's Modulus (GPa)
AZ31-F	138	253	15.0	38.0

temperature on the Instron 5582 at an initial strain rate of 2×10^{-4}/s. The mechanical properties of AZ31-F are shown in Table 2.

2.2. Fatigue crack propagation experiments

L-T orientation compact tension specimens with a width of 50.8 mm and a thickness of 6.35 mm were prepared from the extruded plate of AZ31-F as shown in Fig. 1. The Chevron notch was used for straight crack growth. All specimens were polished with fine sandpaper and Al_2O_3 powders to monitor the crack growth. All FCP tests were conducted on a servo-hydraulic machine in ultra-high vacuum conditions at ambient temperature. The vacuum FCP experiments were conducted in a specially designed ultra-high vacuum chamber mounted on the testing machine, and a schematic illustration of the vacuum test system is shown in Fig. 2. To maintain the dynamic pressure below 1×10^{-7} Torr, a mechanical pump and turbo-molecular pump were used.

The FCP experiments were conducted principally under constant load amplitude, with a sinusoidal frequency of 20 Hz. The FCP rates in the near threshold region were obtained by using the load-shedding technique in accordance with ASTM 647. The range of the stress intensity factor (ΔK) for the CT specimen was calculated as

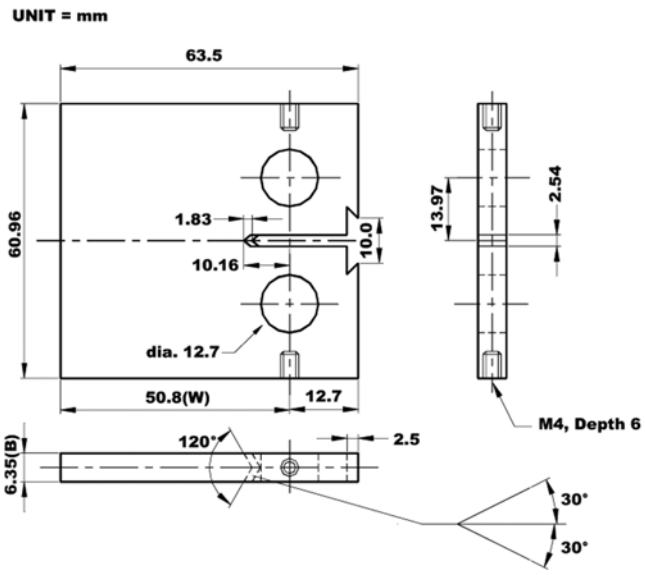

Fig. 1. Schematic illustration of the CT type fatigue specimen.

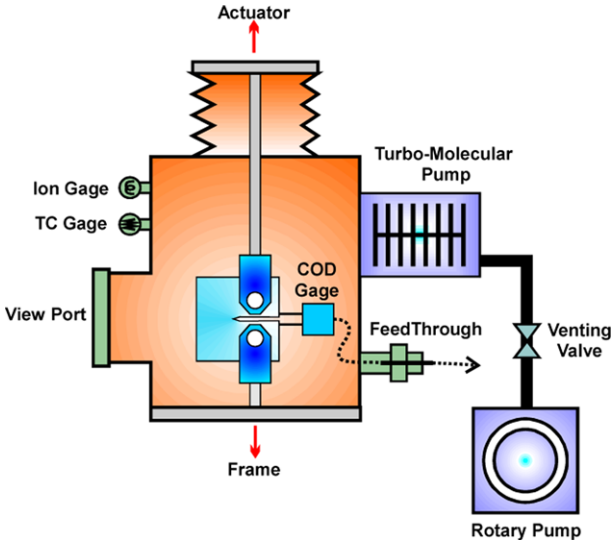

Fig. 2. Schematic illustration of the ultra high vacuum fatigue test system.

$$\Delta K = \frac{\Delta P}{B\sqrt{W}} \frac{(2+a)}{(1-a)^{3/2}} (0.886 + 4.64a - 13.32a^2 + 14.72a^3 - 5.6a^4) \quad (1)$$

where $\Delta P = P_{max} - P_{min}$, P is the load, B is the specimen thickness, W is the specimen width, and a is the crack length. The value of the threshold stress intensity range, ΔK_{th}, was defined as ΔK at da/dN below 1×10^{-10} m/cycle in the present study. To determine the influence of the load ratio, R, on the FCP behavior of the AZ31-F, fatigue tests were conducted at various R ratios of 0.1, 0.3, 0.5, and 0.75. The crack growth was monitored with a traveling telemicroscope. The crack closure loads were determined from a series of load versus displacement plots which were obtained at a reduced frequency of 1 Hz, with a compliance technique using a crack opening displacement (COD) gauge attached to the face of the crack. The crack closure stress intensity factor, K_{cl}, was calculated from the crack closure load, P_{cl}. The fracture surface of the fatigue-tested specimen was examined with a scanning electron microscope (SEM). The average surface roughness on the crack surface was measured from a fractured specimen using a profilometer with a 0.016 μm resolution. The total travel length was 6 mm along the thickness direction of the fractured specimens.

3. RESULTS AND DISCUSSION

The fatigue crack propagation rates of the AZ31 with L-T orientation at various load ratios in an ultra-high vacuum are shown in Fig. 3 as a function of the stress intensity factor range, ΔK. The values for ΔK_{th} of the AZ31-F were 2.01 MPa√m, 1.80 MPa√m, 1.68 MPa√m and 1.64 MPa√m for *R* ratios of 0.1, 0.3, 0.5, and 0.75, respectively. It was found that the values of ΔK_{th} gradually decreased with an increasing *R* ratio, which is in agreement with the previous data [17-20]. This shows that the ΔK_{th} value of Al 2090 and Ti-6Al-4V decreased with an increasing *R* ratio in a vacuum [17-19]. The ΔK_{th} value of AZ61 and AZ91 also decreased with an increasing *R* ratio in air [20]. Generally, the *R* ratio effect on the FCP rates can be explained by the crack closure phenomena.

The crack closure stress intensity factors were determined during the FCP tests. The crack closure level, K_{cl}/K_{max}, which was determined from the measured stress intensity factors at crack closure divided by the maximum stress

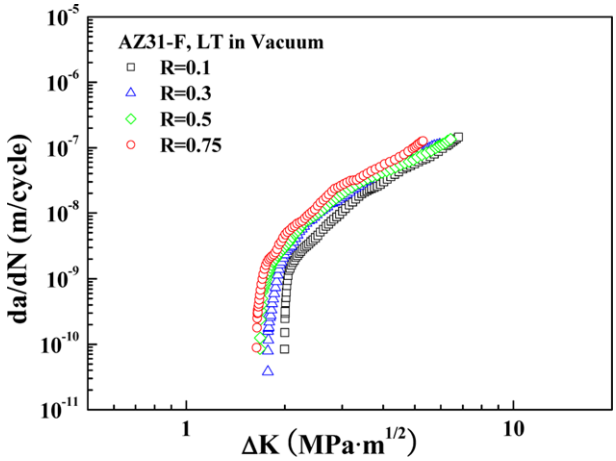

Fig. 3. Effect of the R ratio on the FCP rates of the AZ31-F as a function of ΔK.

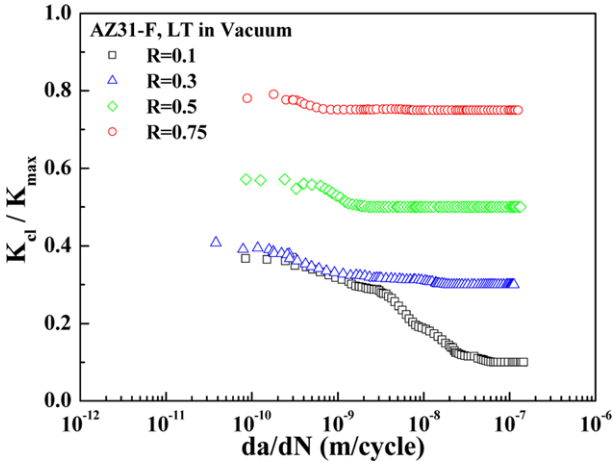

Fig. 4. Crack closure level of the AZ31-F as a function of da/dN.

intensity factors of the AZ31-F with various *R* ratios, was plotted against the crack growth rate in Fig. 4. As shown in Fig. 4, the crack closure levels were high in the near-threshold region, and they decreased with increasing FCP rates at an *R* ratio of 0.1, while the crack closure levels appeared only in the near-threshold region at an *R* ratio of 0.3. In general, the crack closure phenomena significantly affected the FCP behavior in the near-threshold region. Furthermore, the crack closure phenomena decreased with increasing *R* ratio, because the closure phenomena is ineffective as the crack remains open for a larger portion of the cycle at a high *R* ratio.

Since Elber [21] proposed crack closure, extensive studies have been carried out to understand the crack closure effect. Three different kinds of crack closure mechanisms are generally accepted. The first is plasticity-induced crack closure (PICC) caused by the plastic zone, which was proposed by Elber. The second is roughness-induced crack closure (RICC), which is caused by premature contact between asperities at some distance behind the crack tip. The last is oxide-induced crack closure (OICC), in which oxide films are formed near the crack tip in air and are broken by the deformation at the crack tip [22]. Therefore, oxide or corrosion products which are located between the crack faces cause a wedge effect [23]. It is reported that the test environment significantly affects crack closure levels. FCP tests in laboratory air which contains moisture show closure levels which are different from those obtained in a vacuum [16]. In the present study, the FCP tests were conducted in an ultra-high vacuum so that OICC could be excluded.

All of the crack-path morphologies of the AZ31-F tested in vacuum conditions at an *R* ratio of 0.1 are shown in Fig. 5(a). It is reported that crack-path deflection retards FCP rates by reducing the local driving force for FCP and inducing RICC [24]. Nicoletto *et al.* reported that crack paths become tortuous in a coarse grained material and crack branching produces true elastic shielding [25]. The high magnification pictures of crack paths in the near-threshold region and in the high ΔK region are shown in Figs. 5(b) and (c), respectively. The crack path in the near-threshold region is rather straight and shows little plastic deformation on the surface, while that in the high ΔK region meanders and is highly deformed. There is no crack branching phenomena in Fig. 5. The change in the *R* ratio also did not significantly affect the crack path of AZ31-F.

Side views of the fracture surface of the AZ31-F at an *R* ratio of 0.1 with various FCP rates are shown in Fig. 6. The crack propagation direction is from left to right in the micrographs. The degree of crack surface roughness appeared to increase with increasing FCP rate. Fonte *et al.* found that fracture surface roughness is higher in air than that in a vacuum, and the roughness could explain the differences in the FCP rates of medium carbon steel [26]. It was also reported

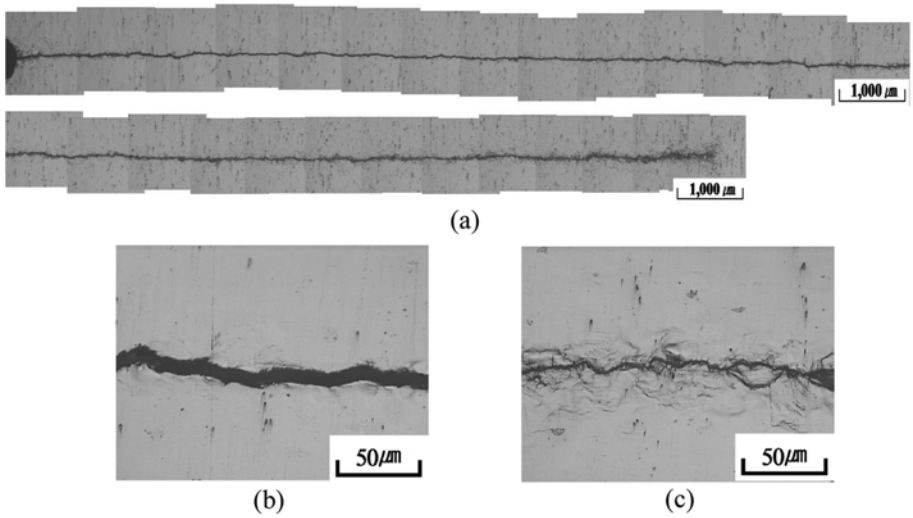

Fig. 5. (a) Crack path morphologies of the AZ31-F tested in vacuum at R=0.1 (b) high magnification picture in the near-threshold region and (c) in the high ΔK region.

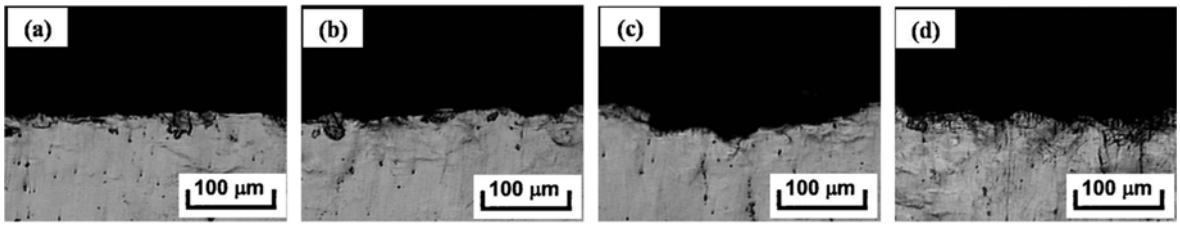

Fig. 6. Side views of the fracture surface of the AZ31-F with different FCP rates at a R ratio of 0.1; (a) da/dN = 1×10^{-10}m/cycle, (b) da/dN = 1×10^{-9}m/cycle, (c) da/dN = 1×10^{-8}m/cycle, (d) da/dN = 1×10^{-7}m/cycle.

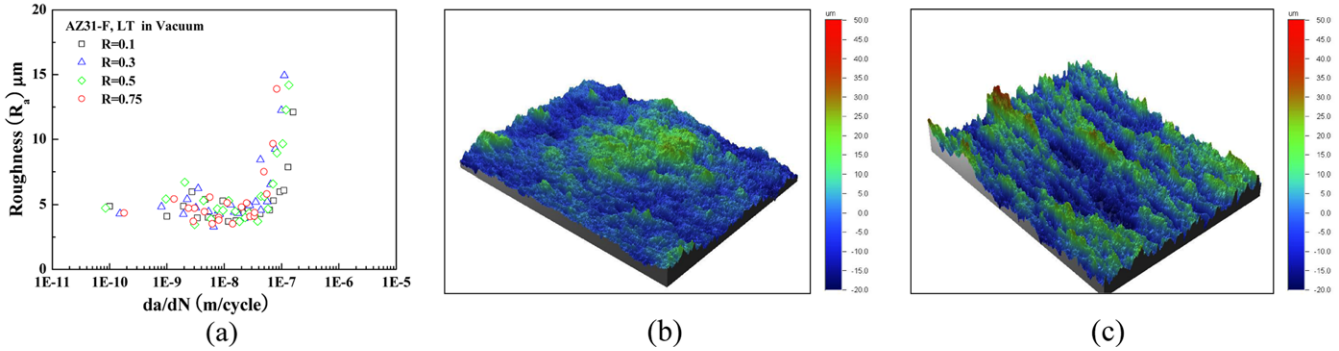

Fig. 7. (a) Roughness of AZ31 as a function of FCG rates in vacuum, (b) 3-D image of roughness of AZ31, L-T, R = 0.75 in vacuum in the near-threshold region and (c) in high ΔK region.

that the enhancement of RICC promotes higher FCP resistance [27]. It is necessary to measure the roughness to understand how much roughness affects the crack closure quantitatively.

The roughness of the AZ3-F with various *R* ratios is shown in Fig. 7. McEvily *et al.* introduced the average fracture surface roughness (R_a) level of the transverse direction to explain the opening stress intensity factor, K_{op}, with ΔK, by using a profilometer with a microscopic scale [28]. The roughness of the near-threshold region and the middle-ΔK region of AZ31 was around 4 μm, but it steeply increased at the high-ΔK region in a vacuum. The roughness difference can be easily seen in Figs. 7(b) and (c), which shows the 3-D roughness image of AZ31-F when *R* is 0.75 in the near-threshold region and in the high-ΔK region in a vacuum, respectively. There is little difference in roughness with different *R* ratios.

Combining the results shown in Figs. 3 and 4, the FCP rates of AZ31-F are shown in Fig. 8 as a function of ΔK_{eff} at various *R* ratios. Comparing the results in Figs. 3 and 8

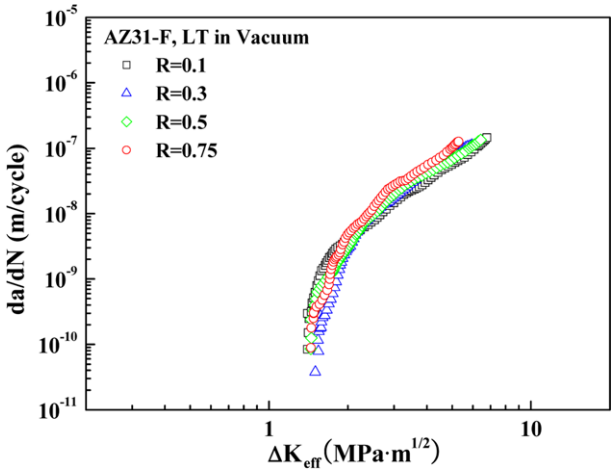

Fig. 8. Effect of the R ratio on the FCP rates of AZ31-F as a function of ΔK_{eff}.

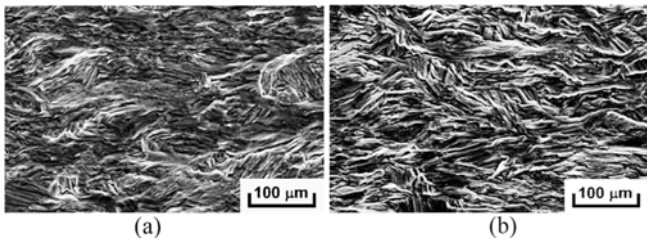

Fig. 9. SEM fractographs of the fatigue-tested AZ31-F obtained at different FCP rates at R=0.1: (a) da/dN = 1×10^{-10}m/cycle and (b) da/dN = 1×10^{-7}m/cycle.

showed that the different FCP curves as a function of ΔK at different *R* ratios converged to a narrow FCP curve when plotted as a function of ΔK_{eff}. The effective threshold stress intensity factor range, $\Delta K_{eff,th}$, showed an almost constant value regardless of the *R* ratio. Therefore, it is concluded that $\Delta K_{eff,th}$ is the intrinsic driving force of the FCP of AZ31-F.

The SEM micrographs of the fatigue-fractured specimens of AZ31-F at an *R* ratio of 0.1 in an ultra-high vacuum are shown in Fig. 9. The crack propagation direction is from left to right in the micrographs. The fracture surface showed mixed quasi-cleavage and trans-granular fracture in the near-threshold region. However, the trans-granular fracture was dominant with increasing FCP rates. It can be expected that the roughness increased with increasing ΔK due to increasing transgranular fracture. There were no corrosion products on the fracture surface due to the ultra-high vacuum.

4. CONCLUSIONS

The following conclusions can be drawn from the present study:

1. The values for ΔK_{th} of the AZ31-F alloy were 2.01 MPa√m, 1.80 MPa√m, 1.68 MPa√m and 1.64 MPa√m for *R* ratios of 0.1, 0.3, 0.5, and 0.75, respectively. The ΔK_{th} value of AZ31-F decreased with increasing *R* ratio.

2. The crack closure levels of AZ31-F were high in the near threshold region.

3. The values of $\Delta K_{eff,th}$, which excluded the crack closure effect, were almost constant and independent of the *R* ratio.

4. The crack closure mechanisms of the AZ31-F in ultra-high vacuum cannot be explained solely by the RICC.

ACKNOWLEDGMENTS

This work was financially supported by the Seoul Research and Business Development Program (10555) and the World Premier Materials (WPM) Program funded by the Ministry of Knowledge Economy through the Research Institute of Advanced Materials.

REFERENCES

1. H. K. Lim, D. H. Kim, J. Y. Lee, J. S. Kyeong, W. T. Kim, and D. H. Kim, *Met. Mater. Int*. **15**, 337 (2009).
2. G. Ben-Hamu, D. Eliezer, K. S. Shin, and L. Wagner, *Cor. Sci. Tech*. **7**, 152 (2008).
3. D. H. Song, C. W. Lee, K. Y. Nam, S. W. Lee, Y. H. Park, I. M. Park, and K. M. Cho, *J. Kor. Inst. Met. & Mater*. **44**, 338 (2006).
4. C. D. Yim, N. E. Kang, and B. S. You, *Met. Mater. Int*. **16**, 377 (2010).
5. S. M. Yin, H. J. Yang, S. X. Li, S. D. Wu, and F. Yang, *Scripta mater*. **58**, 751 (2008).
6. P. K. Liaw, T. R. Leax, V. P. Swaminathan, and J. K. Donal, *Scripta met*. **16**, 871 (1982).
7. A. K. Vasudeven, K. Sadananda, and N. Louat, *Mater. Sci. Eng. A* **188**, 1 (1994).
8. C. S. Lee, S. S. Kim, and K. S. Shin, *Met. Mater*. **3**, 51 (1997).
9. H. E. Kadiri, M. F. Horstemeyer, J. B. Jordon, and Y. Xue, *Metall. Mater. Trans*. A **39**, 190 (2008).
10. R. C. Zeng, Y. B. Xu, W. Ke, and E. H. Han, *Mater. Sci. Eng. A* **509**, 1 (2009).
11. Z. Y. Nan, S. Ishihara, and T. Goshima, *Int. J. Fatigue* **30**, 1181 (2007).
12. Y. Kobayashi, T. Shobusawa, and K. Ishokawa, *Mater. Sci. Eng. A* **234-236**, 220 (1997).
13. B. I. Verkin and N. M. Grinberg, *Mater. Sci. Eng*. **41**, 149 (1979).
14. N. M. Grinverg, *Int. J. Fatigue* **4**, 83 (1982).
15. V. A. Serdyuk and N. M. Grinverg, *Int. J. Fatigue* **5**, 79 (1983).
16. H. C. Jung, C. D. Yim, W. W. Park, C. S. Lee, and K. S. Shin, *Mater. Sci. Forum* **419-422**, 75 (2003).
17. S. S. Kim and K. S. Shin, *Metal. Mater. Trans*. **29A**, 2583 (1998).
18. C. H. Yang, S. S. Kim, C. S. Lee, and K. S. Shin, *J. Kor. Ins. Met. & Mater*. **35**,1302 (1997).

19. E. U. Lee, G. Glinka, A. K. Vasudevan, N. Iyyer, and N. D. Phan, *Int. J. Fatigue* **31**, 1858 (2009).
20. Z. B. Sajuri, Y. Miyashita, and Y. Mutoh, *Mater. Sci. Forum* **419-422**, 81 (2003).
21. W. Elber, *Eng. Fract. Mech*. **2**, 37 (1970).
22. R. C. McClung, *Metall. Trans*. A**22**, 1559 (1991).
23. P. K. Liaw, T. R. Leax, P. S. Williams, and M. G. Peck, *Acta metall*. **30**, 2071 (1982).
24. S. H. Wang and C. Muller, *Mater. Sci. Eng. A* **255**, 7 (1998).
25. G. Nicoletto, R. Konecna, and A. Pirondi, *Fatigue Frac. Engng. Mater. Struct*. **28**, 237 (2005).
26. M. Fonte, F. Romeiro, and M. Freitas, *Int. J. Fatigue*, **29**, 1971 (2007).
27. L. P. Borrego, J. M. Costa, F. V. Antunes, and J. M. Ferreira, *Eng. Failure Analy.* **17**, 11 (2010).
28. A. J. McEvily, M. Renauld, H. Bao, and R. Shover, *Int. J. Fatigue* **19**, 629 (1997).